

## Magnetoelastic transition and negative thermal expansion of $\text{Fe}_2\text{Hf}_{0.83}\text{Ta}_{0.17}$ ribbons

Shen, Qi; Zhang, Fengqi; Dugulan, Iulian; van Dijk, Niels; Brück, Ekkes

**DOI**

[10.1016/j.scriptamat.2023.115482](https://doi.org/10.1016/j.scriptamat.2023.115482)

**Publication date**

2023

**Document Version**

Final published version

**Published in**

Scripta Materialia

**Citation (APA)**

Shen, Q., Zhang, F., Dugulan, I., van Dijk, N., & Brück, E. (2023). Magnetoelastic transition and negative thermal expansion of  $\text{Fe}_2\text{Hf}_{0.83}\text{Ta}_{0.17}$  ribbons. *Scripta Materialia*, 232, Article 115482. <https://doi.org/10.1016/j.scriptamat.2023.115482>

**Important note**

To cite this publication, please use the final published version (if applicable). Please check the document version above.

**Copyright**

Other than for strictly personal use, it is not permitted to download, forward or distribute the text or part of it, without the consent of the author(s) and/or copyright holder(s), unless the work is under an open content license such as Creative Commons.

**Takedown policy**

Please contact us and provide details if you believe this document breaches copyrights. We will remove access to the work immediately and investigate your claim.



## Magnetoelastic transition and negative thermal expansion of $\text{Fe}_2\text{Hf}_{0.83}\text{Ta}_{0.17}$ ribbons

Qi Shen<sup>\*</sup>, Fengqi Zhang, Iulian Dugulan, Niels van Dijk, Ekkes Brück

Fundamental Aspects of Materials and Energy, Faculty of Applied Sciences, Delft University of Technology, Mekelweg 15, Delft 2629 JB, The Netherlands

### ARTICLE INFO

#### Keywords:

Magnetoelastic transition  
Magnetocaloric effect  
Negative thermal expansion  
Mössbauer spectroscopy

### ABSTRACT

In this work, the magnetocaloric effect and negative thermal expansion in melt-spun  $\text{Fe}_2\text{Hf}_{0.83}\text{Ta}_{0.17}$  Laves phase alloys were studied. Compared to arc-melted alloys, which undergo a first-order magnetoelastic transition from the ferromagnetic to the antiferromagnetic phase, melt-spun alloys exhibit a second-order transition. For  $\text{Fe}_2\text{Hf}_{0.83}\text{Ta}_{0.17}$  ribbons, we observed a large volumetric coefficient of negative thermal expansion of  $-19 \times 10^{-6} \text{ K}^{-1}$  over a wide temperature range of 197 – 297 K and a moderate adiabatic temperature change of 0.7 K at 290 K for a magnetic field change of 1.5 T. The magnetic field dependence of the transition temperature ( $dT_t/d\mu_0H = 4.4 \text{ K/T}$ ) for the melt-spun alloy is about half that of the arc-melted alloy (8.6 K/T). The origin of second-order phase transition of the melt-spun alloy is attributed to the partially suppressed frustration effect, which is due to the atomic disorder introduced by the rapid solidification.

The magnetocaloric effect (MCE) is the caloric response to an external magnetic field, characterised in terms of the adiabatic temperature change ( $\Delta T_{\text{ad}}$ ) and the isothermal entropy change ( $\Delta S_m$ ) as performance indices [1,2]. Due to its potentially higher energy efficiency and environmental friendliness compared to vapour compression refrigeration, MCE-based cooling has received considerable attention [3, 4].  $\text{Fe}_2\text{Hf}_{1-x}\text{Ta}_x$  Laves phase materials, as one of the promising MCE candidate systems, has attracted particular interest by the itinerant-electron metamagnetic transition from the ferromagnetic (FM) to the antiferromagnetic (AFM) and then to the paramagnetic (PM) state with increasing temperature at  $x = 0.16 - 0.22$  [5,6]. These compounds crystallize in the hexagonal C14 structure with Fe atoms at two different sites, the 2a site and the 6h site, and Hf/Ta atoms at the 4f site [7,8]. The sharp FM-to-AFM transition is attributed to the fact that the magnetic moment of Fe at the 2a site is frustrated in the AFM state because it lies in the middle between two antiferromagnetically coupled planes [8]. Due to the relatively low heat capacity and frustration effect, a large adiabatic temperature change (3.5 K) was observed for a magnetic field change of 2 T [6], which is comparable to the values for the two well-known MCE materials  $\text{La}(\text{Fe}_{0.88}\text{Si}_{0.12})_{13}\text{H}_y$  [9] and  $\text{Mn}_x\text{Fe}_{2-x}\text{P}_{1-y}\text{Si}_y$  [10]. Accompanied by the magnetoelastic transition, a large negative thermal expansion effect is observed where the volume of the AFM phase is about 1% smaller than that of the FM phase [8].

The common fabrication method for  $\text{Fe}_2(\text{Hf,Ta})$  compounds is arc

melting, followed by annealing at 1272 K for one week [11–13] or without further heat treatment [14,15]. To the best of our knowledge, the melt-spinning technique has not been used to produce  $\text{Fe}_2(\text{Hf,Ta})$  alloys. However, this technique has been shown to have improved magnetocaloric properties in the synthesis of various crystalline magnetocaloric materials such as  $\text{Mn}_{0.66}\text{Fe}_{1.29}\text{P}_{1-x}\text{Si}_x$  [16],  $\text{La}(\text{Fe}_{0.88}\text{Co}_{0.12})_3\text{Si}_x$  [17]  $\text{Gd}_5(\text{SiGeSn})_4$  [18] and  $\text{Ni}_{50.3}\text{Mn}_{35.5}\text{In}_{14.4}$  [19] compared to bulk alloys. The high cooling rate during the solidification process promotes a more homogeneous element distribution, reducing the amount of impurity phase and the annealing time [17,20,21]. Therefore, we have in this study investigated the MCE and the negative expansion effect in a melt-spun  $\text{Fe}_2\text{Hf}_{0.93}\text{Ta}_{0.17}$  alloy and compared it to the arc-melted alloy with the same composition. We found that the melt spinning technique can be an effective method to tune the magnetic field dependence of the transition temperature and to broaden the temperature range for negative thermal expansion applications in  $\text{Fe}_2(\text{Hf,Ta})$  Laves phase compounds.

Polycrystalline  $\text{Fe}_2\text{Hf}_{0.93}\text{Ta}_{0.17}$  compounds were prepared from high-purity elements (Fe 99.98%, Hf 99.7%, Ta 99.9%) by arc melting. To avoid excess Fe atoms occupying the Hf/Ta site, the iron concentration was kept about 0.5% lower than the stoichiometric amount [22,23]. Samples with a total mass of 5 g were melted four or five times, and the button-shaped alloys were flipped over after each melting. The sample without heat treatment is referred to as 'arc-melted Ta0.17'. The sample

<sup>\*</sup> Corresponding author.

E-mail address: [q.shen@tudelft.nl](mailto:q.shen@tudelft.nl) (Q. Shen).

annealed at 1273 K for one week and then quenched into water is noted as ‘annealed Ta0.17’. The sample prepared by melt spinning is noted as ‘melt-spun Ta0.17’. Since there is not much difference in the magnetic properties between the arc-melted and the annealed Ta0.17 alloys, the arc-melted sample without heat treatment is used for comparison with melt-spun sample.

X-ray diffraction (XRD) data were collected with a Panalytical X-Pert PRO using Cu-K $\alpha$  radiation and an Anton Paar TTK 450 temperature chamber. Lattice constants were analysed by Rietveld refinement using the Fullprof software [24]. The magnetic properties at low temperatures (4–370 K) were measured using a superconducting quantum interference device (SQUID) magnetometer model MPMS-XL, equipped with the reciprocating sample option. The ferromagnetic transition temperature  $T_C$  was determined from the temperature derivative of the magnetisation at a magnetic field of 1 T. The  $\Delta S_m$  was calculated from  $M$ - $T$  curves in different magnetic fields using the Maxwell relations. The  $\Delta T_{ad}$  was derived from the calorimetric measurements based on a home-made in-field DSC machine, details can be found in Ref. [25–27]. The microstructure was analysed by Scanning Electron Microscopy (SEM) using a FEI Quanta FEG 450 equipped with energy dispersive X-ray spectroscopy (EDS). Transmission  $^{57}\text{Fe}$  Mössbauer spectra were recorded at different temperatures ranging from 4.2 to 300 K using conventional constant-acceleration or sinusoidal velocity spectrometers with a  $^{57}\text{Co}$  (Rh) source. The velocity calibration was performed using an  $\alpha$ -Fe foil at room temperature. The source and the absorbing samples were kept at the same temperature during cryogenic measurements. The Mössbauer spectra were fitted with the programme Mosswin 4.0 [28].

Fig. 1(a) and (b) show the refined XRD patterns of the arc-melted and melt-spun Ta0.17 alloys at room temperature. They crystallize in the same hexagonal C14 Laves phase structure (space group:  $P6_3/mmc$ ). The refined pattern of the annealed sample is given in Fig. S1(a). The refined lattice parameters are summarized in Table S1. Comparing the XRD patterns of the arc-melted and melt-spun alloys, there is a distinct difference in the relative peak intensity of the three highest peaks, which can be attributed to the different occupation of Hf atoms. For the arc-melted Ta0.17, the Fe atoms are refined to locate at the 2a and the 6h sites and the Hf/Ta atoms at the 4f site. However, the pattern of the melt-spun sample can be fitted better by assuming that part of the Hf atoms

are positioned at the 2a site ( $\chi^2 = 5.13$ ) than by assuming that all the Hf atoms are at the 4f site ( $\chi^2 = 7.43$ ), as shown in Fig. S1(b). This explains the larger volume of the melt-spun alloy ( $171.209 \text{ \AA}^3$ ) compared to that ( $170.013 \text{ \AA}^3$ ) of the arc-melted alloy due to the larger atomic size of the Hf atom (159 pm) than the Fe atom (126 pm). The found occupation of part of the Hf atoms may be caused by the rapid solidification process of the melt-spinning technique. The homogeneity of arc-melted and melt-spun Ta0.17 is compared in SEM images with corresponding line scans (see Fig. 1(c-f)). The SEM images show that the two alloys generally exhibit a single-phase microstructure, although the line scans reveal a compositional variety of about 5 at.%. The somewhat smaller compositional variety in the linear scan of the melt-spun alloy indicates a relatively better homogeneity of the melt-spun alloy compared to the arc-melted alloy.

The magnetic properties of arc-melted, annealed and melt-spun samples were investigated by measuring the  $M$ - $T$  curves in an applied magnetic field of 1 T and the  $M$ - $\mu_0 H$  curves at 5 K. For arc-melted and annealed Ta0.17 alloys, a change in magnetization ( $T_i = 240$  K for the arc-melted alloy and  $T_i = 231$  K for the annealed alloy) corresponds to a magnetic transition with about 2 K thermal hysteresis. The transition is indicated by a weak S-shape for the Arrott-plot in Fig. S2(a) as a first-order transition from the low-temperature FM phase to the high-temperature AFM phase. For the melt-spun alloy, a transition without thermal hysteresis is suggested as a second-order transition ( $T_i = 286$  K) by the absence of a negative slope for the Arrott-plot in Fig. S2(b). The saturation magnetization of annealed Ta0.17 and melt-spun Ta0.17 is about  $52.6 \text{ Am}^2/\text{kg}$ , while that of arc-melted Ta0.17 is  $51.6 \text{ Am}^2/\text{kg}$ . Compared to the arc-melted alloy, the melt-spun alloy exhibits a 46 K higher transition temperature and a slightly higher magnetic anisotropy, which can be attributed to the internal stress introduced during the melt-spinning process [29].

Fig. 2(c) and (d) show the Mössbauer spectra of arc-melted and melt-spun Ta0.17 at 4.2 K and 300 K, respectively. The fitting of the spectra is based on the crystal structure analysis, where Fe has two distinct sites, the 2a and 6h sites, with an atom ratio of 1:3. At 400 K, a typical paramagnetic doublet phase is seen for both alloys (Fig. S3). The fitted Mössbauer data are summarized in Table 1. The similar values of the isomer shift and the quadrupole splitting of both alloys indicate a similar

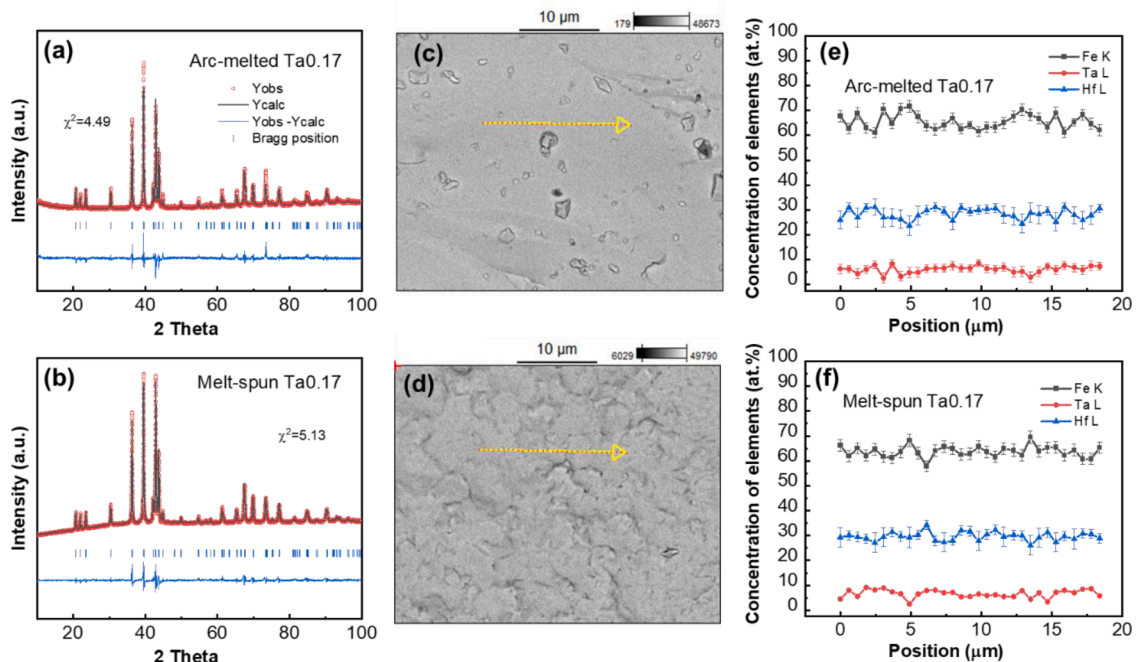
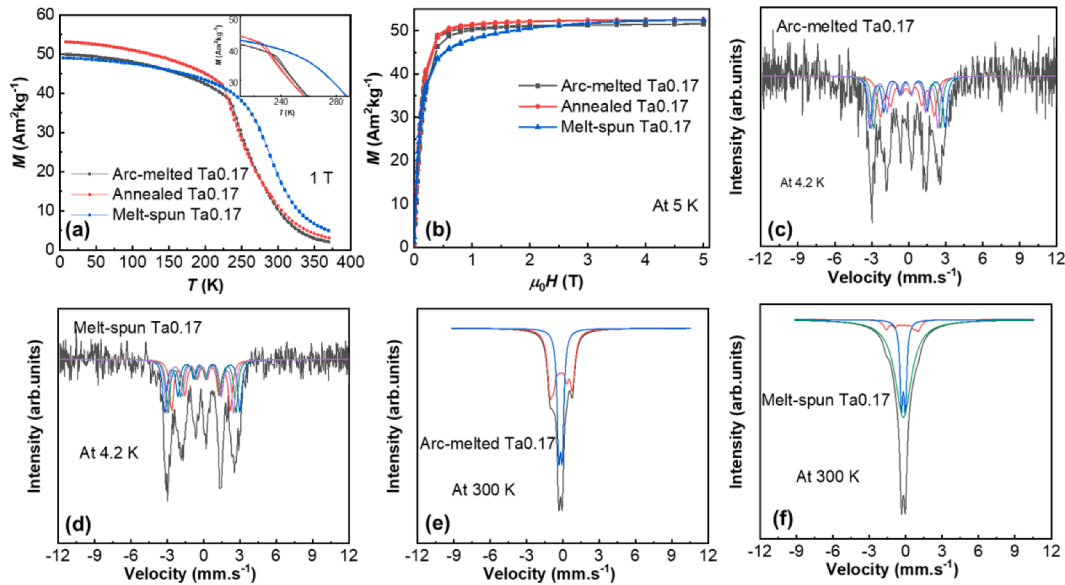


Fig. 1. Rietveld refinement results of the XRD patterns of (a) arc-melted Ta0.17 and (b) melt-spun Ta0.17. SEM images for (c) arc-melted Ta0.17 and (d) melt-spun Ta0.17. Line scan through the yellow line in (c-d) for (e) arc-melted Ta0.17 and (f) melt-spun Ta0.17.



**Fig. 2.** (a)  $M$ - $T$  curves in a magnetic field of 1 T. (b)  $M$ - $\mu_0H$  curves at 5 K. Mössbauer spectra at 4.2 K for (c) arc-melted Ta0.17 and (d) melt-spun Ta0.17. Mössbauer spectra at 300 K for (e) arc-melted Ta0.17 and (f) melt-spun Ta0.17.

**Table 1**

Mössbauer fitted parameters of the arc-melted and melt-spun Ta0.17 alloys, obtained at different temperatures. Experimental uncertainties: Isomer shift: I.S.  $\pm 0.03$  mm s<sup>-1</sup>; Quadrupole splitting: Q.S.  $\pm 0.03$  mm s<sup>-1</sup>; Line width:  $\Gamma \pm 0.05$  mm s<sup>-1</sup>; Hyperfine field:  $\pm 0.2$  T; Spectral contribution:  $\pm 3\%$ .

Sample	Temperature (K)	IS (mm s <sup>-1</sup> )	QS (mm s <sup>-1</sup> )	Hyperfine field (T)	$\Gamma$ (mm s <sup>-1</sup> )	Spectral contribution (phase)
Arc-melted Ta0.17	400	-0.34	0.36	-	0.35	100% (PM)
	4.2	-0.16	0.09	13.6	0.53	25.03% (FM-2a)
		-0.18	0.16	19.0	0.39	24.99% (FM-6h)
		-0.16	0.07	16.8	0.39	24.99% (FM-6h)
		-0.26	-0.12	16.8	0.39	24.99% (FM 6h)
	300	-0.17	0.08	5.77	0.50	58.92% (AFM-6h)
-0.19	0.29	-	0.33	41.08% (AFM-2a)		
Melt-spun Ta0.17	400	-0.33	0.37	-	0.42	100% (PM)
	4.2	-0.17	-0.07	15.1	0.41	25.17% (FM-2a)
		-0.21	0.21	19.3	0.39	24.94% (FM-6h)
		-0.19	0.14	17.4	0.39	24.94% (FM-6h)
		-0.20	-0.14	17.2	0.39	24.94% (FM-6h)
	300	-0.20	-0.17	8.3	0.51	8.42% (AFM-6h)
		-0.19	0.32	-	0.29	21.05% (AFM-2a)
		-0.20	-	-	1.61	70.54% (R)

chemical environment for the 2a and the 6h sites. At 4.2 K, four sextets with the same area are assigned to one 2a site and three 6h sites due to the different reorientation of the spin directions with respect to the principle axis of the electric field gradient [12]. From Table 1, the hyperfine fields of the 2a site and the average 6h site for the melt-spun alloy are slightly larger than those of the arc-melted alloy, which is consistent with the slightly higher saturation magnetization of the melt-spun alloy. This can be related to the larger unit-cell volume for the melt-spun Ta0.17 alloy than the arc-melted Ta0.17 alloy [11]. At 300 K, the arc-melted Ta0.17 alloy is in the AFM state (with no magnetic moment at the 2a site and a small hyperfine field at the 6h site), while the melt-spun Ta0.17 alloy shows a coexistence of a relaxation phase (R) and the AFM phase.

To investigate and compare the evolution of the crystal structure during the magnetic transition, powder X-ray diffraction measurements at different temperatures with a step of 20 K were performed for the arc-melted and melt-spun Ta0.17 alloys. Structure refinement shows that the hexagonal C14 Laves phase structure is maintained over the entire temperature range. A phase coexistence is observed between 217 K – 257 K, further confirming the first-order phase transition in the arc-melted Ta0.17 alloy. The absence of a phase coexistence in melt-spun Ta0.17 alloy confirms the presence of a second-order phase transition.

The refined unit-cell volume and lattice parameters for two alloys are given in Fig. 3(c-f). The arc-melted alloy shows a sharp decrease in unit-cell volume ( $\Delta V/V = -0.4\%$ ) between 237 – 277 K with a negative coefficient of thermal expansion  $\alpha_v \approx -100 \times 10^{-6} K^{-1}$ , comparable to other Fe<sub>2</sub>(Hf,Ta) compounds with a first-order transition [5,7]. The critical change in the thermal expansion curve of the unit-cell volume at 317 K is assigned to the Néel temperature [7], which is consistent with the AFM phase at room temperature in the Mössbauer spectra. On the other hand, the melt-spun alloy exhibits a broad FM-AFM transition accompanied by a lower negative thermal expansion  $\alpha_v = -19 \times 10^{-6} K^{-1}$  within the temperature range of 197 – 297 K. According to the XRD refinement, this broad FM-AFM transition may be caused by the introduced Hf at the 2a site, which to some extent destroys the Kagome layers formed by the Fe atoms occupying the 2a site. Therefore, melt spinning can be an effective method to extend the temperature range for the application of negative thermal expansion in Fe<sub>2</sub>(Hf,Ta) compounds.

To calculate the magnetic entropy change, a series of  $M$ - $T$  curves is measured, as shown in Fig. 4(a) and (b). The magnetic field shifts the transition to higher temperature because the magnetic field favours the FM state.  $\Delta S_m$  is calculated based on Maxwell relations from the  $M$ - $T$  curves. An asymmetric shape of  $\Delta S_m$  is observed with increasing temperature in the arc-melted alloy, while a symmetric shape is present for

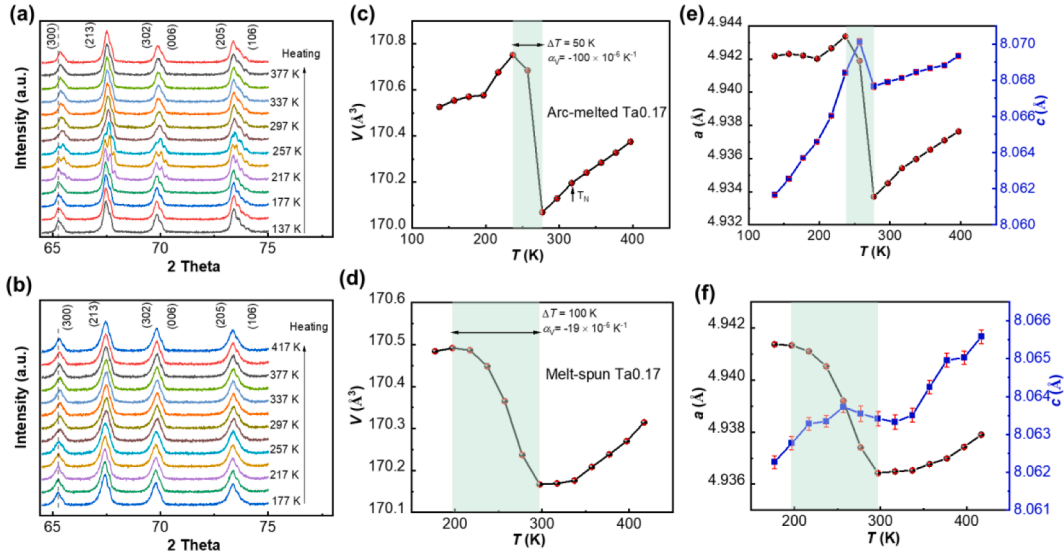


**Fig. 3.** (a, b) XRD patterns as a function of the scattering angle 2 theta, recorded upon heating for a temperature step of 20 K. Temperature dependence of (c, d) unit-cell volume  $V$  and (e, f) lattice parameters  $a$  and  $c$ .

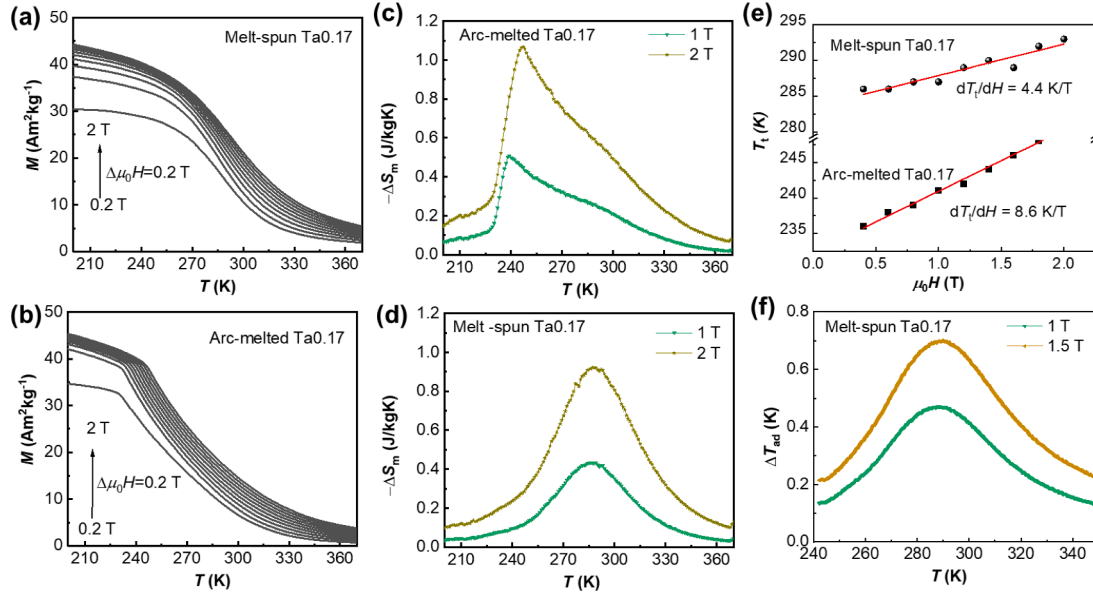


**Fig. 4.**  $M$ - $T$  curves upon heating in different applied magnetic fields for (a) arc-melted Ta0.17 and (b) melt-spun Ta0.17.  $-\Delta S_m$  calculated from the heating curves for (c) arc-melted Ta0.17 and (d) melt-spun Ta0.17. (e)  $T_t$  as a function of magnetic field. (f)  $\Delta T_{ad}$  derived from in-field DSC.

the melt-spun alloy. Both alloys show the same maximum magnetic entropy change of about 1.0 J/kgK for a magnetic field change of 2 T in Fig. 4(c) and (d). However, the magnetic field dependence of the transition temperature  $m = dT_t/d\mu_0H$  is different: 4.4 K/T for the melt-spun alloy and 8.6 K/T for the arc-melted alloy. For the arc-melted Ta0.17 alloy, the value of  $m$  is in good agreement with 7.2 K/T for  $\text{Fe}_2\text{Hf}_{0.825}\text{Ta}_{0.175}$  [30] and 7.7 K/T for  $\text{Fe}_2\text{Hf}_{0.85}\text{Ta}_{0.15}$  [22], which is larger than for other MCE materials with an order-order magnetic transition with 4.6 K/T for  $\text{Mn}_2\text{Sb}_{0.08}\text{Cr}_{0.02}$  [31], but comparable to 9.0 K/T for  $\text{Fe}_{48}\text{Rh}_{52}$  [32]. Although a small  $m$  is required for a maximum adiabatic temperature change at a complete transition, a large  $m$  contributes to the completion of phase transition in a limited magnetic field [33,34]. For different magnetic applications,  $m$  can be tuned by melt-spinning with a suitable solidification rate.

For the melt-spun Ta0.17 alloy,  $\Delta T_{ad}$  is extracted from measurements at a home-made in-field DSC [25–27]. As shown in Fig. 4(f), the value of

$\Delta T_{ad}$  is 0.7 K at 289 K in a magnetic field change of 1.5 T and 0.5 K at 288 K in a magnetic field change of 1 T. The value of  $\Delta T_{ad}$  of the melt-spun Ta0.17 alloy is smaller than that of the arc-melted  $\text{Hf}_{0.84}\text{Ta}_{0.16}\text{Fe}_2$  alloy (3.4 K at the magnetic field change of 1.5 T) [6], which is due to the wide magnetic transition. The coefficient of refrigerant performance (CRP) reflects the MCE performance and can be determined by the following relation:  $\text{CRP} = \frac{|\Delta S_m| \Delta T_{rev}}{\int_0^{\mu_0 H} M(T_C, H) d\mu_0 H}$  [35], where  $\Delta T_{rev}$  is the reversible adiabatic temperature change. Considering  $|\Delta S_m| = 0.5 \text{ J/kgK}$  and  $\Delta T_{rev} = 0.5 \text{ K}$  (taken from in-field DSC measurements) at a magnetic field change of 1 T, the calculated CRP is 0.01, which is smaller than commercial Gd (0.17) [36], but comparable to other second-order phase transition materials such as  $\text{Ni}_{33}\text{Co}_{17}\text{Mn}_{30}\text{Ti}_{20}$  (0.01) [37].

In summary, we have compared the magnetoelastic transition, the microstructure and the magnetocaloric effect in arc-melted and melt-spun  $\text{Fe}_2\text{Hf}_{0.83}\text{Ta}_{0.17}$  compounds. A first-order magnetoelastic phase

transition from the FM to the AFM phase is observed in the arc-melted alloy, while a second-order phase transition is observed in the melt-spun alloy. The same magnetic entropy change of about 1 J/kgK for a magnetic field change of 2 T is obtained for the arc-melted alloy at 247 K and for the melt-spun alloy at 287 K. A thermal hysteresis of 2 K and a phase coexistence in the temperature range 217–257 K is found in the arc-melted alloy. In contrast, the melt-spun alloy undergoes a typical second-order phase transition accompanied by a negative thermal expansion effect with  $\alpha_v = -19 \times 10^{-6} K^{-1}$  over a wide temperature range of 197 – 297 K.

### Declaration of Competing Interest

The authors declare that they have no known competing financial interests or personal relationships that could have appeared to influence the work reported in this paper.

### Acknowledgments

This work is part of the project 'Energy conversion with highly responsive magnetic materials for efficiency' funded by Dutch Research Council with Project no. 680–91–013 and co-financed by Swiss Blue Energy and RSP Technology. The authors thank Anton Lefering, Bert Zwart, Robert Dankelman and Michel Steenvoorden for their technical assistance.

### Supplementary materials

Supplementary material associated with this article can be found, in the online version, at [doi:10.1016/j.scriptamat.2023.115482](https://doi.org/10.1016/j.scriptamat.2023.115482).

### References

- Brück, O. Tegus, D.T. Cam Thanh, N.T. Trung, K.H.J. Buschow, A review on Mn based materials for magnetic refrigeration: structure and properties, *Int. J. Refrig.* 31 (2008) 763–770.
- Gottschall, K.P. Skokov, M. Fries, A. Taubel, I. Radulov, F. Scheibel, D. Benke, S. Riegg, O. Gutfleisch, Making a cool choice: the materials library of magnetic refrigeration, *Adv. Energy Mater.* 9 (2019), 1901322.
- O. Gutfleisch, M.A. Willard, E. Bruck, C.H. Chen, S.G. Sankar, J.P. Liu, Magnetic materials and devices for the 21st century: stronger, lighter, and more energy efficient, *Adv. Mater.* 23 (2011) 821–842.
- V.K. Pecharsky, J. Cui, D.D. Johnson, Magneto)caloric refrigeration: is there light at the end of the tunnel? *Philos. Trans. R. Soc. A* 374 (2016), 20150305.
- L.F. Li, P. Tong, Y.M. Zou, W. Tong, W.B. Jiang, Y. Jiang, X.K. Zhang, J.C. Lin, M. Wang, C. Yang, X.B. Zhu, W.H. Song, Y.P. Sun, Good comprehensive performance of Laves phase  $Hf_{1-x}Ta_xFe_2$  as negative thermal expansion materials, *Acta Mater.* 161 (2018) 258–265.
- Z. Song, Z. Li, B. Yang, H. Yan, C. Esling, X. Zhao, L. Zuo, Large low-field reversible magnetocaloric effect in itinerant-electron  $Hf_{1-x}Ta_xFe_2$  alloys, *Materials* 14 (2021) 1–11.
- B. Li, X.H. Luo, H. Wang, W.J. Ren, S. Yano, C.W. Wang, J.S. Gardner, K.D. Liss, S. H.Lee P.Miao, T. Kamiyama, R.Q. Wu, Y. Kawakita, Z.D. Zhang, Colossal negative thermal expansion induced by magnetic phase competition on frustrated lattices in Laves phase compound  $(Hf,Ta)Fe_2$ , *Phys. Rev. B* 93 (2016), 224405.
- L.V.B. Diop, O. Isnard, E. Suard, D. Benea, Neutron diffraction study of the itinerant-electron metamagnetic  $Hf_{0.825}Ta_{0.175}Fe_2$  compound, *Solid State Commun.* 229 (2016) 16–21.
- A. Fujita, S. Fujieda, Y. Hasegawa, K. Fukamichi, Itinerant-electron metamagnetic transition and large magnetocaloric effects in  $La(Fe_xSi_{1-x})_{13}$  compounds and their hydrides, *Phys. Rev. B* 67 (2003), 104416.
- N.H. Dung, Z.Q. Ou, L. Caron, L. Zhang, D.T.C. Thanh, G.A. de Wijs, R.A. de Groot, K.H.J. Buschow, E. Brück, Mixed magnetism for refrigeration and energy conversion, *Adv. Energy Mater.* 1 (2011) 1215–1219.
- L.V.B. Diop, D. Benea, S. Mankovsky, O. Isnard, Cross over between ferro and antiferromagnetic order in Fe itinerant electron magnetism: an experimental and theoretical study of the model  $(Hf,Ta)Fe_2$  Laves phases, *J. Alloys Compd.* 643 (2015) 239–246.
- Y.J. Huang, S.Z. Li, Z.D. Han, W.X. Wang, Z.Y. Jiang, S.L. Huang, J. Lin, Y.F. Hsia, Mössbauer study of the spin reorientation in pseudobinary alloy  $Hf_{0.82}Ta_{0.18}Fe_2$ , *J. Alloys Compd.* 427 (2007) 37–41.
- Z. Han, D. Wang, S. Huang, Z. Su, S. Tang, Y. Du, Low-field magnetic entropy changes in  $Hf_{1-x}Ta_xFe_2$ , *J. Alloys Compd.* 377 (2004) 75–77.
- S.Y. Dong, X.Z. Yang, J.Y. Chen, Q. Shao, B. Qian, Z.D. Han, C.L. Zhang, X.F. Jiang, Large low-field magnetic entropy changes in as-cast  $Hf_{0.83-x}Zr_xTa_{0.17}Fe_2$  compounds, *Phys. B* 466-467 (2015) 86–89.
- J. Dong, M. Zhang, J. Liu, P. Zhang, A. Yan, Magnetic properties and magnetocaloric effect of  $Hf-Ta-Fe-(Co)$  alloys, *Phys. B* 476 (2015) 171–174.
- Z.Q. Ou, L. Zhang, N.H. Dung, L. van Eijck, A.M. Mulders, M. Avdeev, N.H. van Dijk, E. Brück, Neutron diffraction study on the magnetic structure of  $Fe_2P$ -based  $Mn_{0.66}Fe_{1.29}P_{1-x}Si_x$  melt-spun ribbons, *J. Magn. Magn. Mater.* 340 (2013) 80–85.
- X.B. Liu, X.D. Liu, Z. Altounian, G.H. Tu, Phase formation and structure in rapidly quenched alloys  $La(Fe_{0.88}Co_{0.12})_{13-x}Si_x$  alloys, *J. Alloys Compd.* 397 (2005) 120–125.
- T. Zhang, Y. Chen, Y. Tang, The magnetocaloric effect and hysteresis properties of melt-spun  $Gd_5Si_{1.8}Ge_{1.8}Sn_{0.4}$  alloy, *J. Phys. D* 40 (2007) 5778–5784.
- B. Hernando, J.L. Sánchez Llamazares, J.D. Santos, V.M. Prida, D. Baldomir, D. Serantes, R. Varga, J. González, Magnetocaloric effect in melt spun  $Ni_{50.3}Mn_{35.5}Sn_{14.4}$  ribbons, *Appl. Phys. Lett.* 92 (2008), 132507.
- A. Yan, K.H. Müller, O. Gutfleisch, Structure and magnetic entropy change of melt-spun  $LaFe_{11.57}Si_{1.43}$  ribbons, *J. Appl. Phys.* 97 (2005), 036102.
- Z.Q. Ou, L. Zhang, N.H. Dung, L. Caron, E. Brück, Structure, magnetism and magnetocalorics of Fe-rich  $(Mn,Fe)_{1.95}P_{1-x}Si_x$  melt-spun ribbons, *J. Alloys Compd.* 710 (2017) 446–451.
- Y. Nishihara, Magnetic phase transitions in itinerant electron magnets  $Hf_{1-x}Ta_xFe_2$ , *J. Phys. Soc. Jpn.* 52 (1983) 3630–3636.
- H. Wada, N. Shimamura, M. Shiga, Thermal and transport properties of  $Hf_{1-x}Ta_xFe_2$ , *Phys. Rev. B* 48 (1993) 10221–10226.
- B.H. Toby, R factors in Rietveld analysis: how good is good enough? *Powder Diffraction* 21 (2012) 67–70.
- G. Porcari, M. Buzzi, F. Cugini, R. Pellicelli, C. Pernechele, L. Caron, E. Bruck, M. Solzi, Direct magnetocaloric characterization and simulation of thermomagnetic cycles, *Rev. Sci. Instrum.* 84 (2013), 073907.
- G. Porcari, F. Cugini, S. Fabbri, C. Pernechele, F. Albertini, M. Buzzi, M. Mangia, M. Solzi, Convergence of direct and indirect methods in the magnetocaloric study of first order transformations: the case of Ni-Co-Mn-Ga Heusler alloys, *Phys. Rev. B* 86 (2012), 104432.
- G. Porcari, S. Fabbri, C. Pernechele, F. Albertini, M. Buzzi, A. Paoluzi, J. Kamarad, M. Solzi, Z. Arnold, Reverse magnetostructural transformation and adiabatic temperature change in Co- and In-substituted Ni-Mn-Ga alloys, *Phys. Rev. B* 85 (2012), 024414.
- Z. Klencsar, Mössbauer spectrum analysis by evolution algorithm, *Nucl. Instrum. Meth. B* 129 (1997) 527–533.
- J.A. García, J. Carrizo, L. Elbaile, D. Lago-Cachón, M. Rivas, D. Castrillo, A. R. Pierna, Magnetic anisotropy and magnetostriction in nanocrystalline Fe-Al alloys obtained by melt spinning technique, *J. Magn. Magn. Mater.* 372 (2014) 27–32.
- L.V.B. Diop, M. Amara, O. Isnard, Large magnetovolume effects due to transition from the ferromagnetic to antiferromagnetic state in  $Hf_{0.825}Ta_{0.175}Fe_2$  intermetallic compound, *J. Phys. Condens. Matter* 25 (2013), 416007.
- Q. Shen, I. Batashev, H. Ojiyed, F. Zhang, N. van Dijk, E. Brück, Nonlinear influence of excess Mn on the magnetoelastic transition in  $(Mn,Cr)_2Sb$ , *J. Alloys Compd.* 903 (2022), 164011.
- A.M. Aliev, A.B. Batdalov, L.N. Khanov, A.P. Kamantsev, V.V. Koledov, A. V. Mashirov, V.G. Shavrov, R.M. Grechishkin, A.R. Kaul, V. Sampath, Reversible magnetocaloric effect in materials with first order phase transitions in cyclic magnetic fields:  $Fe_{48}Rh_{52}$  and  $Sm_{0.6}Sr_{0.4}MnO_3$ , *Appl. Phys. Lett.* 109 (2016), 202407.
- J. Liu, T. Gottschall, K.P. Skokov, J.D. Moore, O. Gutfleisch, Giant magnetocaloric effect driven by structural transitions, *Nat. Mater.* 11 (2012) 620–626.
- K.G. Sandeman, Magnetocaloric materials: the search for new systems, *Scr. Mater.* 67 (2012) 566–571.
- E. Brück, H. Yibole, L. Zhang, A universal metric for ferroic energy materials, *Philos. Trans. R. Soc. A* 374 (2016), 20150303.
- M.E. Wood, W.H. Potter, General analysis of magnetic refrigeration and its optimization using a new concept: maximization of refrigerant capacity, *Cryogenics* 125 (1985) 667–683.
- F. Zhang, K. Westra, Q. Shen, I. Batashev, A. Kiecana, N. van Dijk, E. Brück, The second-order magnetic phase transition and magnetocaloric effect in all-d-metal NiCoMnTi-based Heusler alloys, *J. Alloys Compd.* 906 (2022), 164337.